Power System Technology **Volume 46 · Number 2 · 2022**
ISSN: 1000-3673

Multi-target Detection in Substation Scence Based on Attention Mechanism and Feature Balance

Li B., Li Y., Zhu X., Wang S., Qu L., Zeng J., Liu H., Tian Y.

1. Department of Electrical Engineering, School of Applied Technology, University of Science and Technology Liaoning, Anshan, Liaoning 114051, China

2. Ansteel Engineering Technology Corporation Limited, Anshan, Liaoning 114021, China

ABSTRACT

In recent years, the application range of electric energy in modern industry has gradually expanded. Permanent magnet synchronous motor has the characteristics of high efficiency and energy saving and has obvious advantages in traction application. In order to achieve good vector control of permanent magnet synchronous motor in the full speed range, Research on model reference adaptive system (MRAS) and pulsating high frequency injection method to construct the permanent magnet synchronous motor vector control system and combined with the flux weakening control algorithm to control the motor under the condition of limited inverter output, so as to realize the sensorless vector control of the motor in the full speed range. The difference between the estimated value of the algorithm and the actual value is compared on the actual experimental platform to verify the feasibility of the control algorithm. The experimental results show that, under medium and high-speed working conditions, the motor speed and rotor position tracking accuracy of MRAS algorithm is high, and the tracking error is less than 0.01rad. The pulsating high-frequency injection method can accurately track the permanent magnet synchronous motor under low-speed working conditions, the speed error is less than 1n / R / min, and the rotor position error is less than 0.03rad. The static and dynamic performance of the control system is good, It can better deal with the sudden change of motor load. Using MRAS algorithm and pulsating high frequency injection method to control permanent magnet synchronous motor in full speed range is of great significance to improve the speed control performance of permanent magnet synchronous motor.

1. INTRODUCTION

With the transformation of global industrial energy structure, the importance of electric energy in modern industry has gradually increased. As the medium of electromechanical energy conversion, the design and control technology of motor is an important research direction in the field of modern electrical transmission [1, 2]. In the field of railway traction, the high-efficiency and small volume synchronous motor has gradually replaced the traditional asynchronous motor [3, 4]. The permanent magnet synchronous motor uses the permanent magnet to provide the magnetic field, the motor structure is more simplified, the motor rotor volume is smaller, the collector ring and brush structure are omitted, and the operation stability and reliability of the motor are improved [5, 6].

There is no excitation current loss in the application of permanent magnet synchronous motor, which further improves the working efficiency and power density of the motor and has significant advantages in the field of traction application [7, 8]. Railway and other rail transit systems consume a large amount of energy. The use of energy-saving and efficient permanent magnet synchronous motor in railway traction is of great practical significance for the promotion of environmental protection and emission reduction [9, 10]. Therefore, the research and construction of sensorless vector control system of permanent magnet synchronous motor to improve the performance of motor vector control, provide motor technical support for the development of national rail transit, and have long-term value for global energy conservation and emission reduction,

2. DESIGN OF SENSORLESS CONTROL SYSTEM FOR PERMANENT MAGNET SYNCHRONOUS MOTOR

2.1. Motor Mathematical Model Construction and Field Weakening Control

Permanent magnet synchronous motor is developed from the traditional electrically excited synchronous motor, which eliminates the structures such as excitation winding and commutation transposition, introduces the permanent magnet structure, reduces the reactive power exchange between the motor and the power grid, and makes the working performance of the motor more reliable [11, 12]. Permanent magnet synchronous motor is mainly divided into built-in type and surface mounted type. The electromagnetic performance of built-in permanent magnet synchronous motor is salient pole structure, and ferromagnetic material with large permeability is used as the medium between adjacent poles of permanent magnet, while the electromagnetic performance of surface mounted permanent magnet synchronous motor is hidden pole structure [13, 14]. Taking the built-in permanent magnet synchronous motor as the research object, the vector control technology of the built-in permanent magnet synchronous motor is analyzed and studied. Firstly, the mathematical model of the permanent magnet synchronous motor is established, ignoring the electronic hysteresis and eddy current loss, the core reluctance and saturation of the motor stator and rotor, and there is no damping winding on the motor rotor [15, 16]. The back EMF wave of the three-phase winding of the motor is a sine wave. Under static three-phase ABC shafting, the voltage equation of permanent magnet synchronous motor is expressed as follows:

$$u_s^{abc} = R_s i_s^{abc} + \frac{d\psi_s^{abc}}{dt} \tag{1}$$

In equation (1), R_s represents stator resistance, u_s^{abc} represents three-phase stator voltage vector, i_s^{abc} represents three-phase current flux vector, ψ_s^{abc} represents three-phase stator flux vector, t represents time, a, b and c represent ABC axis coordinates, and the three-phase space vector obtained by equivalent transformation of three-phase physical quantities is expressed as follows:

$$\begin{cases} u_s^{abc} = \frac{2}{3}(u_a + au_b + a^2u_c) \\ i_s^{abc} = \frac{2}{3}(i_a + ai_b + a^2i_c) \\ \psi_s^{abc} = \frac{2}{3}(\psi_a + a\psi_b + a^2\psi_c) \end{cases} \tag{2}$$

The rotor magnetic circuit of the built-in permanent magnet synchronous motor is asymmetric, and the motor changes electrically under the influence of rotor position angle [17, 18]. Combined with the double reaction theory of traditional electrically excited synchronous motor, the current, voltage and flux linkage vectors of the motor are converted into rotating coordinate system. The positive direction of axis is the direction of rotor flux linkage space vector, and the positive direction of axis is the direction of axis, rotating 90° counterclockwise. The coordinate conversion is carried out by equal amplitude transformation [12, 13]. The stator magnetic field component equation under shafting is expressed as follows:

$$\begin{cases} \psi_d = L_d i_d + \psi_f \\ \psi_q = L_q i_q \end{cases} \tag{3}$$

In formula (3), $L_d i_d$ and $L_q i_q$ respectively represent the armature reaction generated by the stator current, and L is the motor inductance. The voltage equation under dq shafting is expressed as follows:

$$u_s^{dq} = R_s i_s^{dq} + \frac{d\psi_s^{dq}}{dt} + j\omega_r \psi_s^{dq} \tag{4}$$

The component form of stator voltage equation under dq shafting is shown as follows:

$$\begin{cases} u_d = R_s i_d + L_d \frac{di_d}{dt} - \omega_r L_q i_q \\ u_q = R_s i_q + L_q \frac{di_q}{dt} + \omega_r L_d i_d + e_{back} \end{cases} \tag{5}$$

In equation (5), ω_r represents the electrical angular velocity, $e_{back} = \omega_r \psi_f$represents the back EMF generated by rotor flux linkage ψ_f in the stator equivalent winding, and equation (5) is the basic equation of vector control of permanent magnet synchronous motor. The electromagnetic torque of the motor is expressed as follows:

$$T_e = p\left[\psi_f i_s \sin\delta + \frac{1}{2}(L_d - L_q) i_s^2 \sin 2\delta\right] \tag{6}$$

In equation (6), δ represents the torque angle, that is, the space vector angle between stator current i_s and excitation flux ψ_f. Convert the stator current into dq shafting, and the form of stator current component is as follows:

$$\begin{cases} i_d = i_s \cos\delta \\ i_q = i_s \sin\delta \end{cases} \tag{7}$$

Then the electromagnetic torque of the motor can be expressed as:

$$T_e = 1.5p\left[\psi_f i_s + \left(L_d - L_q\right) i_d i_q\right] = T_{e1} + T_{e2} \tag{8}$$

In equation (8), p is the number of poles, T_{e1} represents the permanent magnet torque generated by the interaction between the permanent magnet flux linkage and the stator current and represents the d-axis current of the motor stator and the reluctance torque generated by the stator under the rotor salient pole structure. The expressions of T_{e1} and T_{e2} are as follows:

$$\begin{cases} T_{e1} = 1.5p\psi_f i_q \\ T_{e2} = 1.5p\left(L_d - L_q\right) i_d i_q \end{cases} \tag{9}$$

It can be seen from equation (9) that the permanent magnet torque and reluctance torque of the motor are directly proportional to the stator q-axis current, and has an impact on the size of the motor stator flux. Therefore, the output torque of the motor can be controlled by adjusting the current of the stator on the d-axis and q-axis, so as to realize the vector control of the motor [19, 20]. The mechanical motion equation of the motor is expressed as follows:

$$J\frac{d\omega_m}{dt} = T_e - T_L - B\omega_m \tag{10}$$

In equation (10), J represents the moment of inertia, ω_m represents the mechanical angular speed of the motor, T_L represents the load torque and B represents the damping coefficient. Under the determined bus voltage, the motor speed has a limit value. In order to ensure that the motor continues to speed up under the limit value, the dynamic flux weakening regulation structure is introduced into the basic structure of vector control to quickly regulate the current of permanent magnet synchronous motor [21, 22]. The flux weakening controller is shown in Figure 1. u_{dref} and u_{qref} represent the stator d-axis reference voltage and q-axis reference voltage respectively, i_{sref} and $i_{sref}^{'}$ represent the stator reference current and adjustable current respectively, and $i_{dref}^{'}$ and $i_{qref}^{'}$ represent the d-axis adjustable current and q-axis adjustable current respectively. Set the inverter output voltage limit $|u_s|_{max}$ to $4U_{dc}/3\sqrt{3}$ to improve the output of motor inverter and make the inverter work under square wave operation. The flux weakening controller is used to adjust the reference value of the motor stator current, increase the stator d-axis negative current, and reduce the stator q-axis current at the same time, so as to keep the stator voltage balanced, so as to realize the further speed increase of the motor.

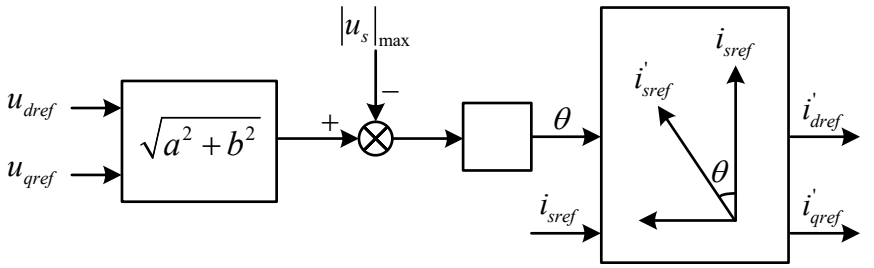

Figure 1 Field weakening controller structure

2.2. Rotor Estimation in Medium and High Speed Section Based on MRAS Algorithm

Model reference adaptive system (MRAS) is developed from modern control theory. It takes the vector control system of permanent magnet synchronous motor as the reference model and the speed as the quantity to be solved [23, 24]. The state equation of the model is expressed as follows:

$$\frac{dx}{dt} = Ax + Bu \tag{11}$$

In equation (11), x represents the system state component, u represents the system input, and B and A are matrix parameters. The stator voltage equation of permanent magnet synchronous motor is expressed as state matrix:

$$\begin{pmatrix} \frac{di_d}{dt} \\ \frac{di_q}{dt} \end{pmatrix} = \begin{pmatrix} -\frac{R_s}{L_d} & -\frac{L_q}{L_d}\omega_r \\ -\frac{L_d}{L_q}\omega_r & -\frac{R_s}{L_q} \end{pmatrix} \begin{pmatrix} i_d \\ i_q \end{pmatrix} + \begin{pmatrix} \frac{u_d}{L_d} \\ \frac{u_q}{L_q} - \frac{\omega_r}{L_q}\psi_f \end{pmatrix} \tag{12}$$

Take the motor current i as the state vector and the voltage as the input vector to replace the variables. Variables i' and u' are expressed as follows:

$$\begin{cases} i' = \begin{pmatrix} i'_d \\ i'_q \end{pmatrix} = \begin{pmatrix} i_d + \frac{\psi_f}{L_d} \\ i_q \end{pmatrix} \\ u' = \begin{pmatrix} u'_d \\ u'_q \end{pmatrix} = \begin{pmatrix} u_d + R_s\frac{\psi_f}{L_d} \\ u_q \end{pmatrix} \end{cases} \tag{13}$$

The current component after substitution is expressed as follows:

$$\begin{cases} i_d' = i_d + \frac{\psi_f}{L_d} = \frac{1}{L_d}\left(L_d i_d + \psi_f\right) = \frac{\psi_d}{L_d} \\ i_q' = \frac{\psi_q}{L_q} \end{cases} \tag{14}$$

$$\begin{cases} \frac{di\prime}{dt} = Ai' + Bu' \\ A = \begin{pmatrix} -\frac{R_s}{L_d} & -\frac{L_q}{L_d}\omega_r \\ -\frac{L_d}{L_q}\omega_r & -\frac{R_s}{L_q} \end{pmatrix}, B = \begin{pmatrix} \frac{1}{L_d} & 0 \\ 0 & \frac{1}{L_q} \end{pmatrix} \end{cases} \tag{15}$$

The adjustable model is constructed according to the state equation of the reference model. Taking ω_r in the state matrix A as the adjustable parameter and the input u' remains unchanged, there is a current estimation value $\hat{\imath}'$ under the adjustable model. The adjustable model is expressed as follows:

$$\begin{cases} \frac{d\hat{\imath}\prime}{dt} = \hat{A}\hat{\imath}' + \hat{B} \\ \hat{A} = \begin{pmatrix} -\frac{R_s}{L_d} & -\frac{L_q}{L_d}\hat{\omega}_r \\ -\frac{L_d}{L_q}\hat{\omega}_r & -\frac{R_s}{L_q} \end{pmatrix}, \hat{B} = \begin{pmatrix} \frac{1}{L_d} & 0 \\ 0 & \frac{1}{L_q} \end{pmatrix} \end{cases} \tag{16}$$

When the current estimated value $\hat{\imath}'$ is consistent with the current value of the reference model, and the state of the adjustable model is the same as that of the reference model, the estimated speed is basically the same as the real speed [25, 26]. Therefore, the estimated speed can be adjusted through the current error to make the speed error zero. Let the current error vector be $e = i' - \hat{\imath}'$ and subtract the reference model from the adjustable model to obtain:

$$\frac{de}{dt} = Ae - J(\hat{\omega}_r - \omega_r)\hat{\imath}' \tag{17}$$

In equation (17), $J = \begin{pmatrix} 0 & -\frac{L_q}{L_d} \\ \frac{L_d}{L_q} & 0 \end{pmatrix}$ and $W = J(\hat{\omega}_r - \omega_r)\hat{\imath}'$ form the standard feedback system of the model. The structure of the standard feedback system is shown in Figure 2.

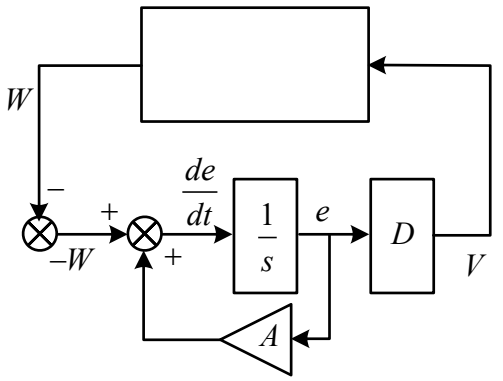

Figure 2 Standard feedback system structure

In unit matrix $D = I$ in Figure 2, due to the short sampling period, it can be considered that the motor speed in adjacent sampling periods is basically the same, so the motor reference model is a linear time invariant system. The output variable $V = e$ of the control system needs a nonlinear time-varying feedback system to analyze the relationship between V and the feedback quantity. The feedback system is an adaptive law. Combined with Popov hyperstability theory, the proportional integral adaptive law is used for analysis, and the adjustable parameters are expressed as follows:

$$\begin{aligned}\hat{\omega}_r &= K_p\varepsilon_i + \int_0^t K_i\varepsilon_i d\tau + \hat{\omega}_r(0) \\ &= \left(K_p + \frac{K_i}{s}\right)\left[\frac{L_q}{L_d} i_d\hat{\imath}_q - \frac{L_d}{L_q} i_q\hat{\imath}_d - \left(\frac{L_q}{L_d} - \frac{L_d}{L_q}\right)\hat{\imath}_d\hat{\imath}_q - \frac{\psi_f}{L_q}\left(i_q - \hat{\imath}_q\right)\right]\end{aligned} \tag{18}$$

In equation (18), K_p and K_i are the proportional gain parameters and integral gain parameters of the control system respectively. The reference model current and adjustable model current are input to the regulator, and the output value is the estimated value of motor speed. In the actual motor control, the motor current components and can be obtained by using the current sensor to collect the three-phase current, and then the coordinate system transformation, while the motor current estimation components and can be obtained by solving the adjustable model equation. The current estimation value of the cycle is expressed as follows:

$$\begin{cases}\hat{\imath}_d^{(n+1)} = \frac{1}{L_d}\left[-R_s\hat{\imath}_d^{(n)} + L_q\hat{\omega}_r^{(n)}\hat{\imath}_q^{(n)} + u_d^{(n+1)}\right]T_{sample} \\ \hat{\imath}_q^{(n+1)} = \frac{1}{L_q}\left[-L_d\hat{\omega}_r^{(n)}\hat{\imath}_d^{(n)} - R_s\hat{\imath}_q^{(n)} + u_q^{(n+1)} - \psi_f\hat{\omega}_r^{(n)}\right]T_{sample}\end{cases} \tag{19}$$

In equation (19), $\hat{\imath}_d^{(n)}$, $\hat{\imath}_q^{(n)}$ and $\hat{\omega}_r^{(n)}$ respectively represent the current component and electrical angular velocity of the previous period, and T_{sample} represents the sampling period.

The interruption period of the system is far less than the mechanical time constant of the motor, and the motor current and speed in adjacent calculation periods remain unchanged. Therefore, the current of this period is solved by using the current value of the previous period, and the estimated speed of the motor rotor in the current period can be obtained by combining the adjustable model current value obtained by integration. The rotor position angle is obtained by integrating the speed to estimate the motor rotor position. The motor rotor position angle is expressed as follows:

$$\hat{\theta}_r^{(n+1)} = \hat{\theta}_r^{(n)} + \hat{\omega}_r^{(n+1)} T_{sample} \tag{20}$$

The actual output voltage u_{dqout} of the inverter is used as the input voltage variable of the motor reference model, and the model input voltage is used as the input voltage of the motor adjustable model. Therefore, it is necessary to accurately obtain the model input voltage $\hat{u}_{dq}$ as the data premise of MRAS algorithm. The traditional model input voltage acquisition mainly adopts reference type and sampling type. The reference type directly inputs the inverter output reference voltage into the model, but there is a large deviation between the reference voltage and the actual point voltage at low switching frequency, which affects the estimation results of MRAS algorithm [27, 28]. The sampling type samples the three-phase voltage and obtains the input voltage through coordinate transformation. There is a certain phase delay and there is a large demand for sampling resources, which increases the workload of the control system [29, 30]. Therefore, the voltage reconstruction technology is used to obtain the input voltage of the model, which can not only reduce the error between the input voltage and the actual situation, but also avoid increasing the burden of the control system and improve the accuracy of motor rotor estimation. Set the model sampling ratio as n, and there are sampling cycles in the motor switching cycle. At the end of the switching cycle, the small calculation cycle will calculate the duty cycle of pulse width modulation (PWM) wave in the next cycle to complete the update of the corresponding timer register. At the beginning of the switching cycle, based on the updated duty cycle, the phase voltage values of the three phases in the n sampling cycles in the switching cycle are directly given, and the input voltage through the coordinate conversion model is obtained. The voltage reconstruction technology is shown in Figure 3.

Set the sampling ratio, as shown in sampling period 1 and sampling period 5. When the PWM wave in the switching period is low level, the actual motor stator voltage value is 0. As shown in sampling period 3, when the PWM waves in the switching period are high level, DC bus voltage is the actual stator voltage value of the motor. As shown in sampling period 2 and sampling period 4, when the level of PWM wave is switched in the switching period, the average voltage needs to be calculated according to the action time of high level and low level as the input voltage of the model. Suppose the high-level time in the sampling period is and the average voltage is calculated as follows:

$$U_{av} = U_{dc} \cdot \frac{T_{high}}{T_{sample}} + 0 \cdot \left(1 - \frac{T_{high}}{T_{sample}}\right) = \frac{T_{high}}{T_{sample}} U_{dc} \tag{21}$$

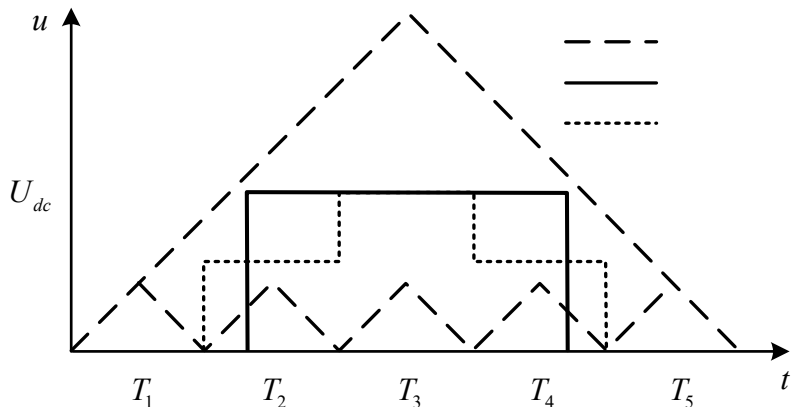

Figure 3 Voltage Reconfiguration Technology

2.3. Low Speed Rotor Estimation Based on High Frequency Voltage Injection

MRAS algorithm establishes the rotor estimation model based on the motor stator voltage equation and uses the back EMF to predict the rotor speed of the motor. It has advantages in the estimation of rotor position and speed under medium and high-speed operating conditions [31]. However, when the permanent magnet synchronous motor is running at low speed, the rotor speed is small, and its back electromotive force is also small. At low speed, the MRAS algorithm is used to estimate the motor rotor speed, the estimation error is large, and the motor vector control accuracy becomes worse [32, 33]. Therefore, the research adopts the way of high-frequency voltage signal injection, adds additional excitation signal at the voltage output of the inverter, extracts the high-frequency response to obtain the rotor speed information, and accurately estimates the rotor speed and position of the motor at low speed. A high-frequency sinusoidal voltage signal is injected into the estimated $\hat{d}\hat{q}$ shaft system of the motor by using the pulsating voltage injection method, and then the high-frequency component of the current at the output end is solved to obtain the speed and position information of the motor rotor. The high-frequency voltage signal is injected into the $\hat{d}$ shaft as follows:

$$\begin{cases} u_h^{\hat{d}} = U_h \cos \omega_h t \\ u_h^{\hat{q}} = 0 \end{cases} \tag{22}$$

Let $\Delta\theta_r = \theta_r - \hat{\theta}_r$ be the angular deviation between the real dq -axis system and the estimated $\hat{d}\hat{q}$-axis system, then the motor state matrix under $\hat{d}\hat{q}$-axis system is expressed as follows:

$$\begin{bmatrix} \frac{di_h^{\hat{d}}}{dt} \\ \frac{di_h^{\hat{q}}}{dt} \end{bmatrix} = \begin{pmatrix} \cos\Delta\theta_r & -\sin\Delta\theta_r \\ \sin\Delta\theta_r & \cos\Delta\theta_r \end{pmatrix} \begin{pmatrix} \frac{1}{L_d} & 0 \\ 0 & \frac{1}{L_q} \end{pmatrix} \begin{pmatrix} \cos\Delta\theta_r & \sin\Delta\theta_r \\ -\sin\Delta\theta_r & \cos\Delta\theta_r \end{pmatrix} \begin{bmatrix} U_h \cos\omega_h t \\ 0 \end{bmatrix} \tag{23}$$

The current component under the $\hat{d}\hat{q}$ shafting is expressed as follows:

$$\begin{cases} i_h^{\hat{d}} = \left[\frac{U_h}{\omega_h}\left(\frac{cos^2\,\Delta\theta_r}{L_d} + \frac{sin^2\,\Delta\theta_r}{L_q}\right)\right] sin\,\omega_h\,t \\ i_h^{\hat{q}} = \left[\frac{U_h}{\omega_h}\left(\frac{1}{L_d} - \frac{1}{L_q}\right) sin(2\Delta\theta_r)\right] sin\,\omega_h\,t \end{cases} \tag{24}$$

In equation (24), $sin(2\Delta\theta_r)$ is the motor rotor angle error signal, and the error signal is on the amplitude of the -axis current signal. ω_h represents the center angular frequency. The demodulation is realized by multiplying the -axis current by after passing through the band-pass filter of ω_h:

$$\begin{aligned} i_h^{\hat{q}} \cdot sin\,\omega_h\,t &= \left[\frac{U_h}{\omega_h}\left(\frac{1}{L_d} - \frac{1}{L_q}\right) sin(2\Delta\theta_r)\right] \cdot sin^2\,\omega_h\,t \\ &= \left[\frac{U_h}{\omega_h}\left(\frac{1}{L_d} - \frac{1}{L_q}\right) sin(2\Delta\theta_r)\right] \cdot (1 - cos\,2\,\omega_h t) \end{aligned} \tag{25}$$

Pass the signal through the low-pass filter, remove the frequency doubling component in the signal, retain the DC component, set the amplitude $K_r = \frac{U_h}{\omega_h}\left(\frac{1}{L_d} - \frac{1}{L_q}\right)$, and the error signal is expressed as follows:

$$\varepsilon_r = \frac{U_h}{\omega_h}\left(\frac{1}{L_d} - \frac{1}{L_q}\right) sin\,2\left(\theta_r - \hat{\theta}_r\right) \approx 2K_r\left(\theta_r - \hat{\theta}_r\right) \tag{26}$$

The proportional integral regulator is used to process the error signal to obtain the estimated value of rotor speed, and the estimated value of rotor position angle is obtained after integral processing. The operation flow of pulsating voltage injection method is shown in Figure 5. Collect the three-phase current of the motor for park transformation, convert the three-phase current from ABC shafting to -axis shafting, and extract the signal in combination with -axis current to estimate the rotor speed and position of the motor at low speed.

The research combines MRAS algorithm with pulsating high-frequency injection method to form the composite sensorless control system of permanent magnet synchronous motor in medium high-speed state and low-speed state. The algorithm switching between medium high-speed section and low-speed section is realized by hysteresis switching, and the smooth switching between the two algorithms is realized by setting hysteresis interval. Based on flux weakening control, the vector control of permanent magnet synchronous motor in the full speed range is realized by using MRAS algorithm and pulsating high-frequency injection method. The vector control system of permanent magnet synchronous motor is shown in Figure 4. The outer loop of the control system is speed loop controller, and the inner loop is current loop controller. A double loop control system is formed by controlling the motor rotor speed and stator current.

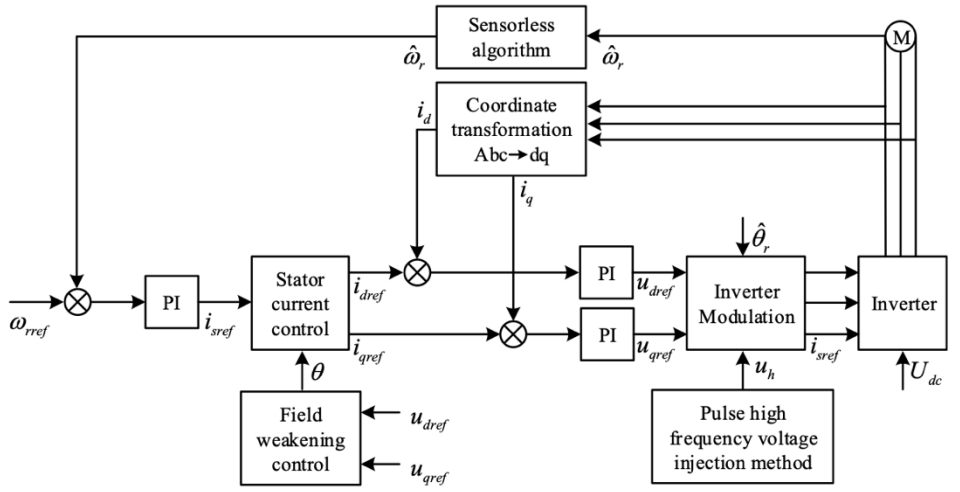

Figure 4 Vector control system of permanent magnet synchronous motor

3. VECTOR CONTROL EFFECT ANALYSIS

3.1. Effectiveness Analysis of Field Weakening Control

In order to verify the effectiveness and practicability of the designed flux weakening control system of permanent magnet synchronous motor, the relevant software programs of permanent magnet synchronous motor are built on the experimental hardware platform. The hardware circuit is a three-phase two-level topology. The parameters of the experimental platform are shown in Table 1.

Table 1 Experimental parameters

Parameter	Parameter value
Stator resistance	0.025Ω
Stator d-axis inductance	0.7645mH
Stator q-axis inductance	2.1377mH
Rotor flux linkage	0.2335Wb
Polar logarithm	4
Inverter bus voltage	350V
Rated current	135A
Rated voltage	233.5V
Rated power	45kW
Switching frequency	10kHz

Make the motor load 100 N·m, compare the actual data with the reference model data, and compare the motor speed response data, motor stator shaft current data, motor reference current and output torque data. The control effect of permanent magnet synchronous motor under flux weakening control is shown in Figure 5,

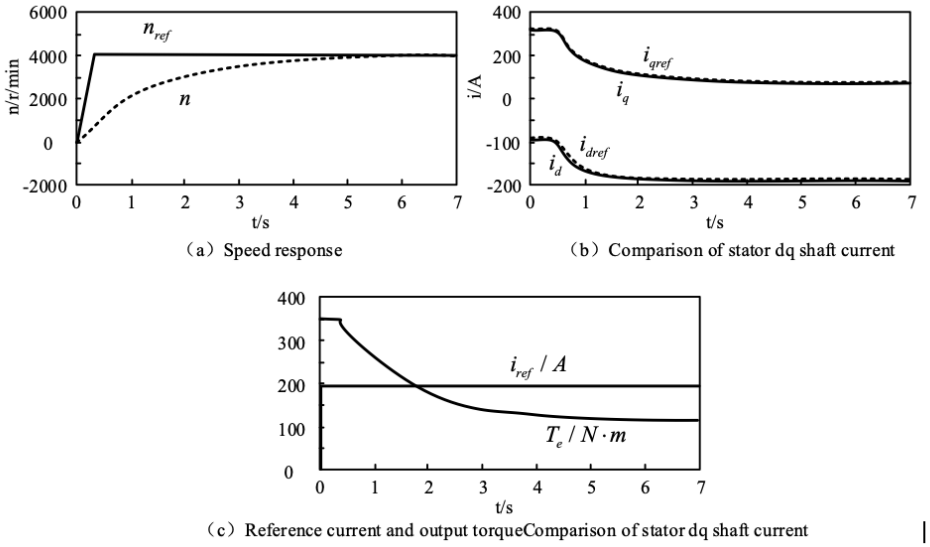

（a）Speed response

（b）Comparison of stator dq shaft current

（c）Reference current and output torqueComparison of stator dq shaft current

Figure 5 Control effect of permanent magnet synchronous motor under flux weakening control

As can be seen from Figure 5, in the time of 0 to 0.5 s, the motor speed is in the range of 0 to 150 r/min, the motor inverter output is not limited, the motor reference current reaches the maximum level, and the output torque of the motor is also the maximum value. The output torque remains constant. At this time, the motor is in the constant torque working state. When the motor speed exceeds 1500 r/min at 0.5, the inverter output is limited. The field weakening control module is used to control the motor, increase the d-axis negative current of the motor and reduce the q-axis current of the motor. With the increase of motor speed, the motor output torque gradually decreases, and the motor is in constant power working state. In the process of motor speed-up after 0.5 s, the response speed of the control system is fast, the transition between the two working states is smooth, and there is no impact. The flux weakening control module can effectively complete the vector control of the motor when the output of the motor inverter is limited. The flux weakening control algorithm is effective in the vector control of permanent magnet synchronous motor.

3.2. Analysis of Motor Rotor Estimation Results

In order to verify the effectiveness of the vector control system of permanent magnet synchronous motor in medium and high speed section based on MRAS algorithm, the estimated data of motor rotor speed and position under medium and high speed conditions are compared with the actual data. The waveforms of the actual and estimated values of motor speed and rotor position under 1000r/min speed are shown in Figure 6.

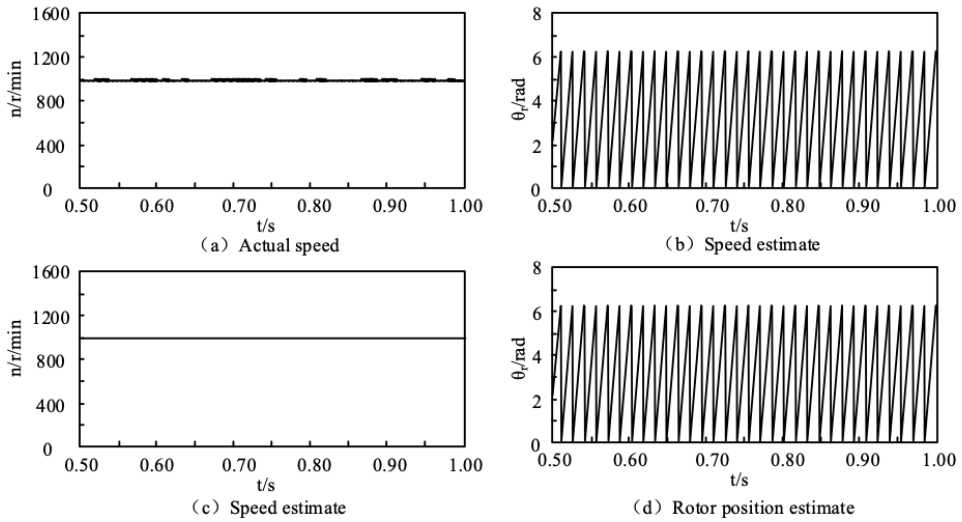

Figure 6 Actual and estimated values of motor speed and rotor position at 1000 r/min

As can be seen from Figure 6, under the working condition of 1000 r/min, MRAS algorithm can accurately track the motor speed and rotor position, and the rotor position tracking error value is less than 0.01 rad, which basically ensures the real-time and accurate tracking of the rotor speed and position of permanent magnet synchronous motor. In order to verify the feasibility of the quality control system of low-speed permanent magnet synchronous motor based on pulsating high-frequency injection method, the estimated data of motor speed and rotor position under low-speed working condition are compared with the actual data. The waveform of the actual value and estimated value of motor speed and rotor position at 50 r/min is shown in Figure 7.

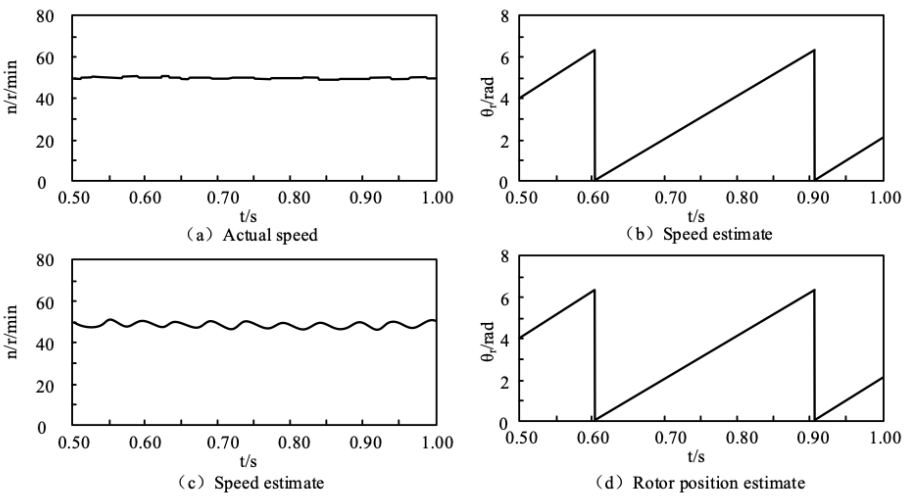

Figure 7 Actual and estimated values of motor speed and rotor position at 50 r/min

As can be seen from Figure 7, under the working condition of 50 r/min, the motor vector control using the pulsating high-frequency injection method can realize the accurate tracking of the motor rotor speed and position. The rotor position tracking error is less than 0.03 rad, the motor speed tracking error is less than 1 n/r/min, and the tracking accuracy is high. The signal extraction process of pulsating high-frequency injection method involves two-step signal processing. When the current signal is filtered by band-pass filter and low-pass filter, there will also be the problem of phase lag, resulting in the increase of estimation error. In order to verify the dynamic performance stability of MRAS algorithm and pulsating high-frequency injection method, apply a sudden load of 100 N·m after 1 s of operation, analyze the tracking waveform of MRAS algorithm under 1000 r/min condition and the tracking waveform of pulsating high-frequency injection method under 50 r/min condition. The changes of sudden load waveform under the control of the two algorithms are shown in Figure 8.

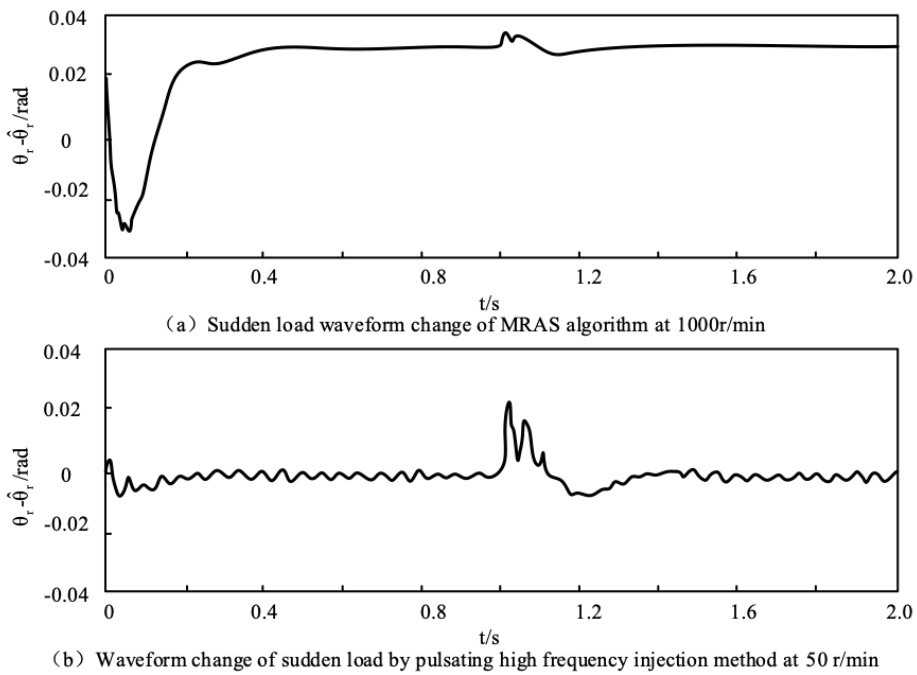

（a）Sudden load waveform change of MRAS algorithm at 1000r/min

（b）Waveform change of sudden load by pulsating high frequency injection method at 50 r/min

Figure 8 Waveform change of sudden load controlled by two algorithms

As can be seen from Figure 8, when the motor is running at high speed and low speed, the load is suddenly added, and the error curves of the two algorithms fluctuate, but tend to be stable within 0.2 S. MRAS algorithm and pulsating high-frequency injection method can quickly adapt to the sudden change of load, track the motor speed and rotor position quickly and accurately, and the control system has good dynamic and static performance, which can better deal with complex actual working conditions.

4. CONCLUSION

In the application of modern electric drive industry, the traditional position sensor has been difficult to meet the requirements of modern industry. In order to improve the vector control performance of permanent magnet synchronous motor in the full speed range, the MRAS algorithm and pulsating high-frequency injection method are studied to carry out the position sensor free vector control of permanent magnet synchronous motor, and the method of flux weakening control is adopted when the output is limited, the motor vector control in the full speed range is realized. The experimental results show that the flux weakening control system has fast response speed, can realize the smooth conversion between constant torque and constant power, and has good motor control effect when the inverter output is limited. MRAS algorithm can accurately track the motor under high-speed working conditions, and the tracking error is less than 0.01rad.

Pulsating high-frequency injection method can accurately track the point motor under low-speed operation, with rotor position error less than 0.03rad and speed error less than 1n/r/min. moreover, the dynamic performance of the two algorithms is good, which can better deal with the sudden change of motor load. Working conditions have an impact on the accuracy of MRAS algorithm, and the research has not deeply discussed different working conditions. In the future, the rotor estimation under light load and heavy load conditions can be studied separately.

REFERENCES

[1] Chen, J. and Y. Zhang, Dual-Vector Model Predictive Current Control of Permanent Magnet Synchronous Motor Drives with the Segment Golden Search Method. IEEE Access, 2020. 8: p. 183826-183846.

[2] Li, C., T.N. Shi, Y. Yan, Z.Q. Zhou, and C.L. Xia, Predictive control with optimal vector sequence for permanent magnet synchronous motors. Journal of Power Electronics, 2020. 20(2): p. 553-565.

[3] Niu, S., Y. Luo, W. Fu, and X.D. Zhang, An Indirect Reference Vector Based Model Predictive Control for a Three-Phase PMSM Motor. IEEE Access, 2020. 8: p. 29435 – 29445.

[4] Zhao, B., H. Li, and J. Mao, Double-objective finite control set model-free predictive control with DSVM for PMSM drives. Journal of Power Electronics, 2019. 19(1): p. 168-178.

[5] Li, G., J. Hu, Y. Li, and J. Zhu, An Improved Model Predictive Direct Torque Control Strategy for Reducing Harmonic Currents and Torque Ripples of Five-Phase Permanent Magnet Synchronous Motors. IEEE Transactions on Industrial Electronics, 2019. 66(8): p. 5820-5829.

[6] Yang, C., Z. Che, and L. Zhou, Composite Feedforward Compensation for Force Ripple in Permanent Magnet Linear Synchronous Motors. Journal of Shanghai Jiaotong University (Science), 2019. 24(6): p. 782-788.

[7] Li, S., H. Won, X. Fu, M. Fairbank, D.C. Wunsch, and E. Alonso, Neural-Network Vector Controller for Permanent-Magnet Synchronous Motor Drives: Simulated and Hardware-Validated Results. IEEE Transactions on Cybernetics, 2019. 50(7): p. 3218 - 3230.

[8] Zheng, Z. and D. Sun, Model Predictive Flux Control with Cost Function-Based Field Weakening Strategy for Permanent Magnet Synchronous Motor. IEEE Transactions on Power Electronics, 2019. 35(2): p. 2151-2159.

[9] Kuang, Z., S. Wu, B. Du, H. Xu, S. Cui, and C.C. Chan, Thermal Analysis of Fifteen-Phase Permanent Magnet Synchronous Motor Under Different Fault Tolerant Operations. IEEE Access, 2019. 7: p. 81466-81480.

[10] Wang, S., D. Peng, and Z. Wu, Embedded Position Detection for Permanent Magnet Synchronous Motor with Built-In Magnets. IEEE Sensors Journal, 2019. 19(21): p. 9818-9825.

[11] Khiabani, A.G. and A. Heydari, Optimal Torque Control of Permanent Magnet Synchronous Motors Using Adaptive Dynamic Programming. IET Power Electronics, 2020. 13(12): p. 2442-2449.

[12] Baneira, F., J. Doval-Gandoy, A.G. Yepes, and O. Lopez, DC-Current Injection with Minimum Torque Ripple in Interior Permanent-Magnet Synchronous Motors. IEEE Transactions on Power Electronics, 2020. 35(2): p. 1176-1181.

[13] Lee, K. and Y. Han, MTPA Control Strategy Based on Signal Injection for V/f Scalar-Controlled Surface Permanent Magnet Synchronous Machine Drives. IEEE Access, 2020. 8: p. 96036 - 96044.

[14] Xu, Y., X. Ding, J. Wang, and Y. Li, Three-vector-based low-complexity model predictive current control with reduced steady-state current error for permanent magnet synchronous motor. IET Electric Power Applications, 2020. 14(2): p. 305-315.

[15] Deng, W., X. Fu, and W. Xie, Reduction of Common-Mode Voltage in Matrix Convert-Fed Permanent Magnet Synchronous Motor System with Rotating Vectors. IEEE Access, 2020. 8: p. 205894-205901.

[16] Xie, M. and L. Xie, Decoupling Control of Permanent Magnet Synchronous Motor with Support Vector Regression Inverse System Method. IEEE Access, 2020. 8: p. 212687-212698.

[17] Chen, Z., H. Zhang, W. Tu, G. Luo, D. Manoharan, and R. Kennel, Sensorless Control for Permanent Magnet Synchronous Motor in Rail Transit Application Using Segmented Synchronous Modulation. IEEE Access, 2019. 7: p. 76669-76679.

[18] Cui, K., C. Wang, L. Gou, and Z. An, Analysis and Design of Current Regulators for PMSM Drives Based on DRGA. IEEE Transactions on Transportation Electrification, 2020. 6(2): p. 659-667.

[19] Lu, W., D. Zheng, Y. Lu, K. Lu, L. Guo, W. Yan, and J. Luo, New Sensorless Vector Control System with High Load Capacity Based on Improved SMO and Improved FOO. IEEE Access, 2021. 9: p. 40716-40727.

[20] Lee, K.W. and S.I. Kim, Dynamic Performance Improvement of a Current Offset Error Compensator in Current Vector-Controlled SPMSM Drives. IEEE Transactions on Industrial Electronics, 2019. 66(9): p. 6727-6736.

[21] Anuchin, A., A. Dianov, and F. Briz, Synchronous Constant Elapsed Time Speed Estimation Using Incremental Encoders. IEEE/ASME Transactions on Mechatronics, 2019. 24(4): p. 1893 - 1901.

[22] Qu, L., W. Qiao, and L. Qu, An Enhanced Linear Active Disturbance Rejection Rotor Position Sensorless Control for Permanent Magnet Synchronous Motors. IEEE Transactions on Power Electronics, 2020. 35(6): p. 6175-6184.

[23] Volosencu, C., Reducing Energy Consumption and Increasing the Performances of AC Motor Drives Using Fuzzy PI Speed Controllers. Energies, 2021. 14(8): p. 2083.

[24] Kesavan, P., and A. Karthikeyan, Electromagnetic Torque-Based Model Reference Adaptive System Speed Estimator for Sensorless Surface Mount Permanent Magnet Synchronous Motor Drive. IEEE Transactions on Industrial Electronics, 2020. 67(7): p. 5936-5947.

[25] Song, Z., J. Yang, X. Mei, T. Tao, and M. Xu, Deep reinforcement learning for permanent magnet synchronous motor speed control systems. Neural Computing and Applications, 2021. 33(5): p. 1-10.

[26] Zhang, Z.F., Y. Wu, and S.Y. Qi, Diagnosis method for open-circuit faults of six-phase permanent magnet synchronous motor drive system. IET Power Electronics, 2020. 13(15): p. 3305-3313.

[27] Hu, P., D. Wang, S. Jin, Y. Wei, C. Chen, N. Lin, Q. Zhang, X. Wu, H. Zhu, and F. Sun, The Modified Model of Third-Harmonic Shaping for a Surface-Mounted Permanent-Magnet Synchronous Motor Under Parallel Magnetization. IEEE Transactions on Industry Applications, 2020. 56(5): p. 4847-4856.

[28] Parvathy, M.L., K. Eshwar, and V.K. Thippiripati, A modified duty-modulated predictive current control for permanent magnet synchronous motor drive. IET Electric Power Applications, 2021. 15(1): p. 25-38.

[29] Qin, X.F., and J.X. Shen, Split ratio optimisation of high-speed permanent magnet synchronous motor with multi-physics constraints. IET Electric Power Applications, 2020. 14(12): p. 2450-2461.

[30] Zhao, S., X. Huang, Y. Fang, and H. Zhang, DC-link-Fluctuation-Resistant Predictive Torque Control for Railway Traction Permanent Magnet Synchronous Motor in Six-Step Operation. IEEE Transactions on Power Electronics, 2020. PP (99): p. 10982 - 10993.

[31] El-Sousy, F., M.M. Amin, and O.A. Mohammed, Robust Optimal Control of High-Speed Permanent-Magnet Synchronous Motor Drives via Self-Constructing Fuzzy Wavelet Neural Network. IEEE Transactions on Industry Applications, 2020. PP (99): p. 999 - 1013.

[32] Petkar, S.G., and T.V. Kumar, computationally efficient model predictive control of three-level open-end winding permanent-magnet synchronous motor drive. IET Electric Power Applications, 2020. 14(7): p. 1210-1220.

[33] Lin, C.H. Linear permanent magnet synchronous motor drive system using AAENNB Control system with error compensation controller and CPSO. Electrical Engineering, 2020. 102(5): p. 1311-1325.